

# Visualizing undyed microplastic particles and fibers with plasmon-enhanced fluorescence

**Wei, Xin-Feng; Rindzevicius, Tomas; Wu, Kaiyu; Bohlen, Martin; Hedenqvist, Mikael; Boisen, Anja; Hakonen, Aron**

*Published in:*
Chemical Engineering Journal

*Link to article, DOI:*
10.1016/j.cej.2022.136117

*Publication date:*
2022

*Document Version*
Publisher's PDF, also known as Version of record

Chemical Engineering Journal 442 (2022) 136117

Contents lists available at ScienceDirect

Chemical Engineering Journal

journal homepage: www.elsevier.com/locate/cej

# Visualizing undyed microplastic particles and fibers with plasmon-enhanced fluorescence

Xin-Feng Wei [a,b], Tomas Rindzevicius [c], Kaiyu Wu [d], Martin Bohlen [a], Mikael Hedenqvist [b], Anja Boisen [c], Aron Hakonen [e,f,*]

[a] Department of Polymers and Composites, RISE Research Institutes of Sweden, SE–501 15 Borås, Sweden
[b] Department of Fibre and Polymer Technology, School of Engineering Sciences in Chemistry, Biotechnology and Health, KTH Royal Institute of Technology, SE–100 44 Stockholm, Sweden
[c] Center for Intelligent Drug Delivery and Sensing Using Microcontainers and Nanomechanics (IDUN), Department of Health Technology, Technical University of Denmark, Kongens Lyngby 2800, Denmark
[d] National Key Laboratory of Science and Technology on Micro/Nano Fabrication, Department of Micro/Nano Electronics, Shanghai Jiao Tong University, 200240 Shanghai, China
[e] Department of Chemistry, Biomaterials and Textiles, RISE Research Institutes of Sweden, SE–501 15 Borås, Sweden
[f] Sensor Visions AB, SE-455 22 Hisings Backa, Sweden

ARTICLE INFO

*Keywords:*
Microplastics
Analysis methods
Water samples
Plasmonic nanostructures
Enhanced fluorescence

ABSTRACT

Despite widespread awareness that enormous consumption of plastics is not sustainable, the global production and use of plastics continue to grow. This generates vast amounts of plastic waste and microplastics, ending up e.g., in the marine environment. There are serious challenges in detecting and measuring microplastics, especially in highly diluted natural samples. Here, a new alternative microplastic detection method based on plasmon-enhanced fluorescence (PEF) was developed and tested using fluorescence microscopy. In particular, gold nanopillar-based substrates, displaying (i) high electromagnetic field enhancement, and (ii) surface superhydrophobicity and high adhesion properties, were utilized to enhance the fluorescence emission signal from microplastics in water samples. The fluorescence microscopy imaging revealed remarkable fluorescence enhancement by the PEF substrates on the microplastic particles and fibers with different sizes of both conventional, low-density polyethylene, and biodegradable poly (butylene adipate-co-terephthalate). The limit of detection and quantification by this method was estimated to be as low as 0.35 and 1.2 femtograms, respectively. The observed fluorescence enhancement of the gold nanopillar substrates for the microplastics was ca. 70 times greater than the case of having the microplastics on a glass substrate. Additionally, 3D FEM simulations were performed to further investigate the system's electromagnetic field distribution near the nanostructures. This new method makes undyed microplastics visible in fluorescence microscopy, even particles and fibres too small to be imaged with conventional light microscopy. This can be a great tool for microplastic research, helping us to detect, study, understand microplastic dynamics in water based systems.

## 1. Introduction

The global plastic production, use, and waste generation are at an all-time high, with a production exceeding 368 million metric tons (Mt) per year [1]. As of 2015, approximately 8300 Mt of virgin plastics had been produced and 6300 Mt of plastic waste had been generated, 79% of which was accumulated in landfills or ended up in natural environments such as rivers, lakes, and often finally in the world's oceans [2]. Another recent contribution to global plastic waste is due to the COVID-19 pandemic and consequent rise in utilization of single-use medical equipment such as gloves, masks, and test kits [3]. Microplastics, defined as plastic particles or fibers with a size less than 5 mm, originating from manufacturing plastics (primary sources) and the degradation of plastic wastes (secondary sources), have become an emerging global concern [4–8]. Their persistence in the environment is estimated to be hundreds or even thousands of years, depending on the type of plastic and their habitats [9]. Recently, the presence of microplastics has been recognized in many unexpected substances/matrices such as in

* Corresponding author at: Department of Chemistry, Biomaterials and Textiles, RISE Research Institutes of Sweden, SE–501 15 Boras, Sweden.
*E-mail address:* aron@sensorvisions.se (A. Hakonen).

https://doi.org/10.1016/j.cej.2022.136117
Received 1 February 2022; Received in revised form 15 March 2022; Accepted 28 March 2022
Available online 30 March 2022

drinking water and bottled water [10,11], human placenta [12] and gentoo penguins (*Pygoscelis papua*) from the remote and pristine Antarctic region [13]. Microplastics are abundant and generated in high numbers anywhere macroscopic plastics are present [14,15]. For example, 25,000 microplastic particles are released from one disposable plastic cup into one cup of hot water in 15 min [16]. Microplastics are prone to accumulate in the environment and pose a significant risk to ecosystems globally [17–21]. For instance, microplastics enriched with organic pollutants and trace metals can be ingested by different organisms and consequently contaminate food chains [22]. Organic pollutants are not only the primary additives used in plastic products, they are also adsorbed or absorbed by the microplastics from the surroundings [23], causing potential toxic effects for numerous bio-organisms [24].

Improved detection of microplastics in various sample matrices is essential for the understanding of microplastic dynamics in natural environments and maybe most of all in natural waters [25]. Common techniques include microscopy (e.g. optical, scanning and transmission electron, atomic force) for physical characterization of their shape, size, and numbers, and spectroscopic analysis (Fourier transform infrared and Raman) for chemical identification based on vibrational information from chemical bonds [26–28]. The presence of a variety of natural particles such as sediments with the same size range as microplastics poses a major challenge in the analysis of environmental matrices through visual inspection using normal optical microscopy [26–28]. In view of this, fluorescence microscopy can be a useful tool in distinguishing microplastic from inorganic particles. However, most plastics do not have high enough intrinsic fluorescence for a clear observation under fluorescence light excitation and microplastic samples usually need to be stained using fluorescent dyes, such as Nile Red, before the observation with fluorescence microscopy [29,30].

On the other hand, substrates that consist of plasmonic metal nanoparticles have been shown to enhance the fluorophore emission intensity by several orders of magnitude, a phenomenon called plasmon-enhanced fluorescence (PEF) or surface-enhanced fluorescence (SEF) [31–35]. The enhancement is mainly attributed to the much larger absorption and scattering cross-sections of the plasmonic nanostructures than that of molecular fluorophores [31,34]. The fluorescence enhancement by plasmonic nanostructured substrates is of value for detecting minute amounts of weakly emitting analytes and species, with an improved limit of detection, and a shorter analysis time; especially for analytes and species which are not detectable by conventional single-molecule fluorescence techniques [31,34,36–39]. PEF is a member of the family of surface-enhanced spectroscopy techniques together with surface-enhanced Raman scattering (SERS) [40,41]. The SERS methodology has been used recently to significantly enhance the detection signal of microplastics and nanoplastics [22,42,43].

In line with SERS, also the PEF techniques have potential advantages in the detection of microplastic samples, since microplastics usually have very weak intrinsic fluorescence, are tiny in size and may occur at low concentrations, for instance in water samples. In this study, PEF substrates were employed for the first time to facilitate the detection of microplastics using fluorescence microscopy. The previously developed gold nanopillar (AuNP) substrates that have been optimized for SERS measurements [44,45], were utilized in this study. The substrates have other interesting properties apart from the beneficial plasmonic properties [44]; for example, the AuNP surface can be tailored to display superhydrophobic and highly adhesive properties, which enables concentrating the samples before analysis [46,47]. Microplastics of both conventional low-density polyethylene (LDPE) as well as biodegradable poly (butylene adipate-co-terephthalate) (PBAT) in MilliQ water samples were placed on the PEF substrates and examined in an optical/fluorescence microscope. LDPE is one of the most used plastics, and PBAT, a semi-aromatic polyester, has been regarded as a promising biodegradable alternative to LDPE, especially in applications of mulch films and plastic shopping bags [48]. Two optical filters with different excitation and emission wavelengths were employed to reveal the fluorescence emission of microplastics that were placed on PEF substrates. The morphology of microplastics on the substrate was also examined using scanning electron microscopy. The fluorescence enhancement factor by the PEF substrates, as well as the limit of detection and quantification, were determined, and 3D Finite-Element-Method (FEM) simulations were performed to understand the underlying mechanisms of the AuNP substrate for PEF. Besides, epoxy microplastics, one of the commonly detected microplastics in oceans (released from boat paints), were also tested using this method. The results present a new method/tool to visualize microplastics in fluorescence microscopy without dying for detecting, studying, understanding microplastics in nature.

## 2. Experimental section

### 2.1. Materials

PBAT with a trademark of Ecoflex® F Blend C1200 and LDPE with a trademark of LUPOLEN 2420 K was purchased from BASF (Germany) and ALBIS (Sweden), respectively. A curing epoxy system with a low viscosity epoxy resin (Araldite LY 1564/Aradur 22962) was purchased from Huntsman (the USA).

### 2.2. Microplastic sample preparation

PBAT and LDPE microplastics in water samples prepared in the previous work were used [48]. The details of sample preparation are described in ref [48]. In brief, extruded PBAT and LDPE films were aged/exposed to MilliQ water and artificial seawater at 23 °C for up to 10 weeks, and microplastics were formed and released into the water samples during the exposure. Epoxy microplastics were prepared by crushing a glass fiber-reinforced epoxy composite plate which was manufactured by vacuum infusion and cured according to supplier recommendation. The obtained microplastics were then added in MilliQ water for further investigation.

### 2.3. AuNP substrate preparation

AuNP substrates were produced as described in ref [45], and are also commercially available from Silmeco ApS (Danmark). In short, vertically standing silicon (Si) nanopillar structures (~50 nm in diameter, ~600 nm in height) on a 6 in. Si wafer were obtained via the Si reactive ion etching (RIE) process using $SF_6$ and $O_2$ gases, followed by 1 min $O_2$-plasma cleaning. Next, a gold metal film (200 nm thick) was deposited on the Si nanopillar structure using electron-beam evaporation at a 1 nm/s deposition rate. Finally, the wafer was diced into single 3x3 mm chips using a laser micromachining tool (3D-Micromac AG, D-09126 Chemnitz, Germany). The AuNP substrates were kept in a desiccator (250–280 mbar) for a minimum of 4 weeks prior to the experiments.

### 2.4. Method development of using PEF substrates for microplastic detection

The sampling procedure, described in ref [49], involved placing a 2 μl droplet of a microplastic containing water sample on the AuNP substrate, and then allowing the water to evaporate in a cleanroom environment, before microscopy measurements. An upright Olympus BX 63 microscope, equipped with an Olympus DP72 cooled color camera and 2.5x/0.08, 5x/0.15, 10x/0.30, 20x/0.45 and 50x/0.8 objectives, were used to detect the microplastics placed on the AuNP substrate. U-FUN and U-MWBV2 optical filters, which have excitation and emission filters BP 360 – 370 nm / LP420 nm and BP 400 – 440 nm / LP 475 nm, respectively, were used for fluorescence observation. The number of samples was: 12 PBAT, 8 LDPE, 2 Epoxy, which was the number of evaporated and analyzed sample droplets. For PBAT and LDPE type more than 100 fluorescence images was acquired. Similarly, some

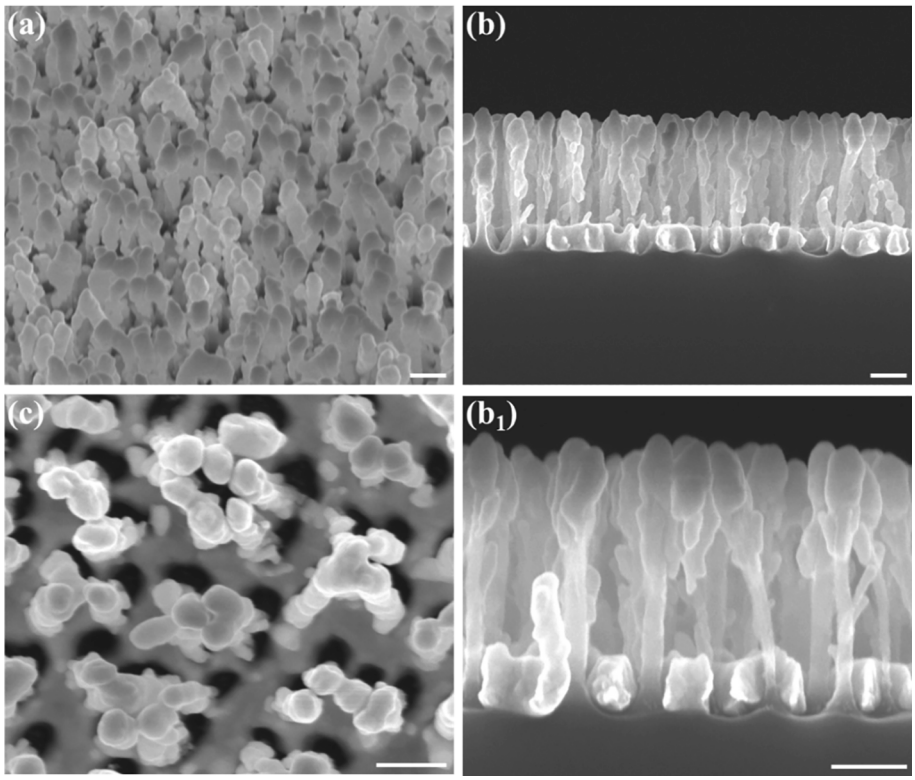


**Fig. 1.** SEM images of the gold nanopillar substrates viewed from a 45° angle (a), side (b, $b_1$), and top (c). Scalebars are 200 nm long.

microplastic sample droplets were evaporated on microscope glass slides and analyzed for comparison.

The intrinsic fluorescence from the pristine PBAT and LDPE plastic films (fabricated as described in ref [48]) was measured in a 60°angle to minimize Rayleigh scattering into the detector. Excitation/emission matrix scans were performed in 200 – 600 nm ranges, with a 2.00 nm slit widths, on a Horiba Fluoromax 4 instrument. Specific emission scans were selected from the matrix scans.

### 2.5. Scanning electron microscopy (SEM)

Scanning electron microscopy (SEM) characterization of the gold nanopillar substrates was performed using a Zeiss Supra 40 VP field emission scanning electron microscope (Jena, Germany). SEM analysis of the microplastics placed on the gold nanopillar substrates was performed after the water evaporation from the initially placed 2 μl microplastic-containing droplets.

### 2.6. Simulation

3D FEM simulations were performed using COMSOL MULTIPHYSICS version 5.5. The electromagnetic field distribution near the nanostructures was calculated by solving scattering fields in series. A flat surface port located at the top of the solution domain was used to excite linearly polarized incident electromagnetic fields. A perfectly matched layer was employed to eliminate nonphysical reflections. The model geometry of the nanopillar was drawn from the information in SEM images. For simplicity, and to reduce calculation time, gold caps were modelled as ellipsoids. The minimum gap distance between adjacent nanopillars was 2 nm. Materials were modeled by refractive indices as a function of wavelength [50]. The structures were placed in a vacuum environment.

## 3. Results and discussion

### 3.1. Gold nanopillar substrates

Fig. 1 shows the structure of the employed plasmonic AuNP substrates. The gold nanopillars are 750 nm in height, and ca. 50 and 100 nm in diameter for the bottom and top parts, respectively. The substrates can be characterized as a superhydrophobic AuNP surface, i.e. water placed on the surface forms droplets with a large contact angle and a small contact area [46]. Water droplets are also strongly adhered by the mechanism of elasto-capillarity, which pulls the water down into the substrate by capillary forces. At the same time, the liquid drying process pulls the gold-capped Si pillars closer into micro-sized clusters, which, due to the inter-particle localized surface plasmon-resonance coupling, enhances the electromagnetic field and forms the so-called electromagnetic hot spots [46,47]. Due to the mechanism of elasto-capillarity water is pulled down between the gold nanopillars, resulting in some nanopillars being pulled together while others are pulled apart by capillary forces. Likely, larger polymer particles and fibres can interact better at pulled apart locations, while smaller can interact good everywhere, but possibly the best nanopillar interaction and fluorescence enhancement can be achieved at pulled together locations.

Overall, the AuNP substrates display several advantageous properties. Firstly, the NP-based SERS-active substrates have shown to yield SERS enhancement factors of up to $10^8$ and uniformity of the SERS signal intensity across a 3x3 mm surface below 10% RSD [47]. In addition, the surfaces are contaminant-free due to the fabrication in the cleanroom environment [44,45]. Secondly, the NP-based substrates have a superhydrophobic surface leading to a minimal droplet imprint on the surface and a high local concentration of non-volatiles after evaporation [47]. Thirdly, despite the fact that the NP surfaces have superhydrophobic properties, the substrates also show a very high adhesion of water droplets, hence generating elasto-capillarity effects that pull the flexible nanopillars into clusters forming multiple electromagnetic hot spots [46]. Furthermore, the AuNP substrates can yield fluorescence

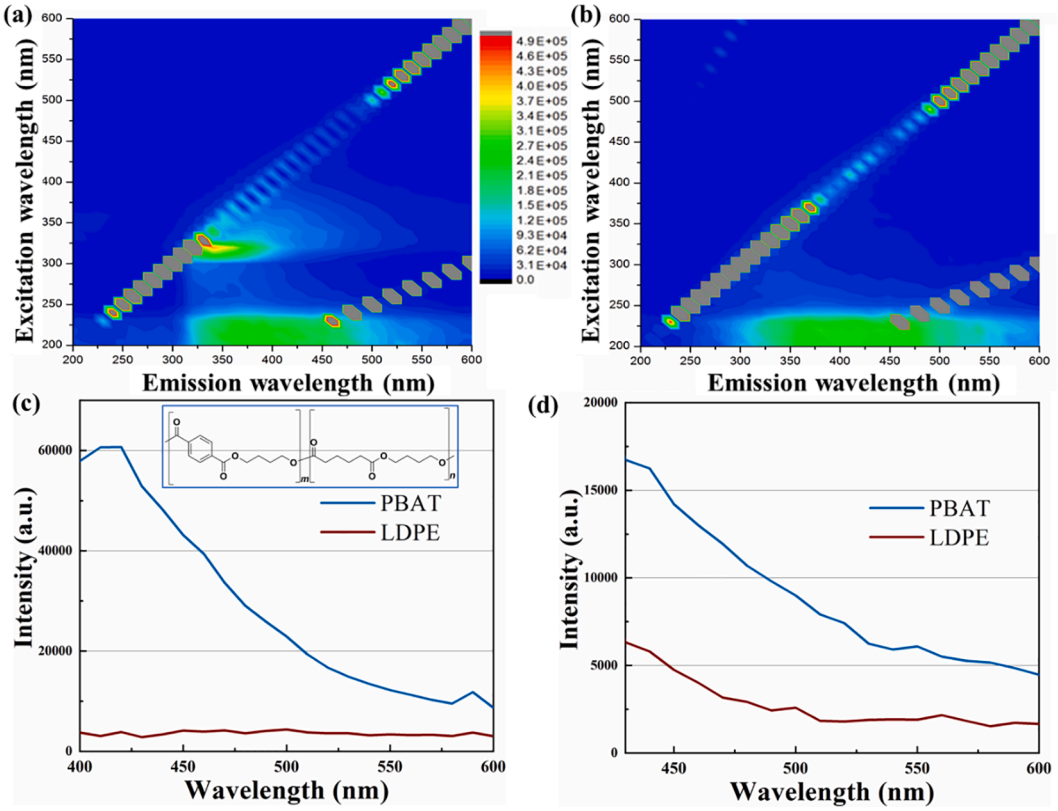


**Fig. 2.** Fluorescence matrix scans of (a) PBAT and (b) LDPE films, and specific fluorescence emission scans for the plastics with excitations at (c) 360 nm and (d) 400 nm, which are wavelengths relevant for the employed optical filters in the fluorescence microscopy. Insert in c shows the molecular structure of PBAT.

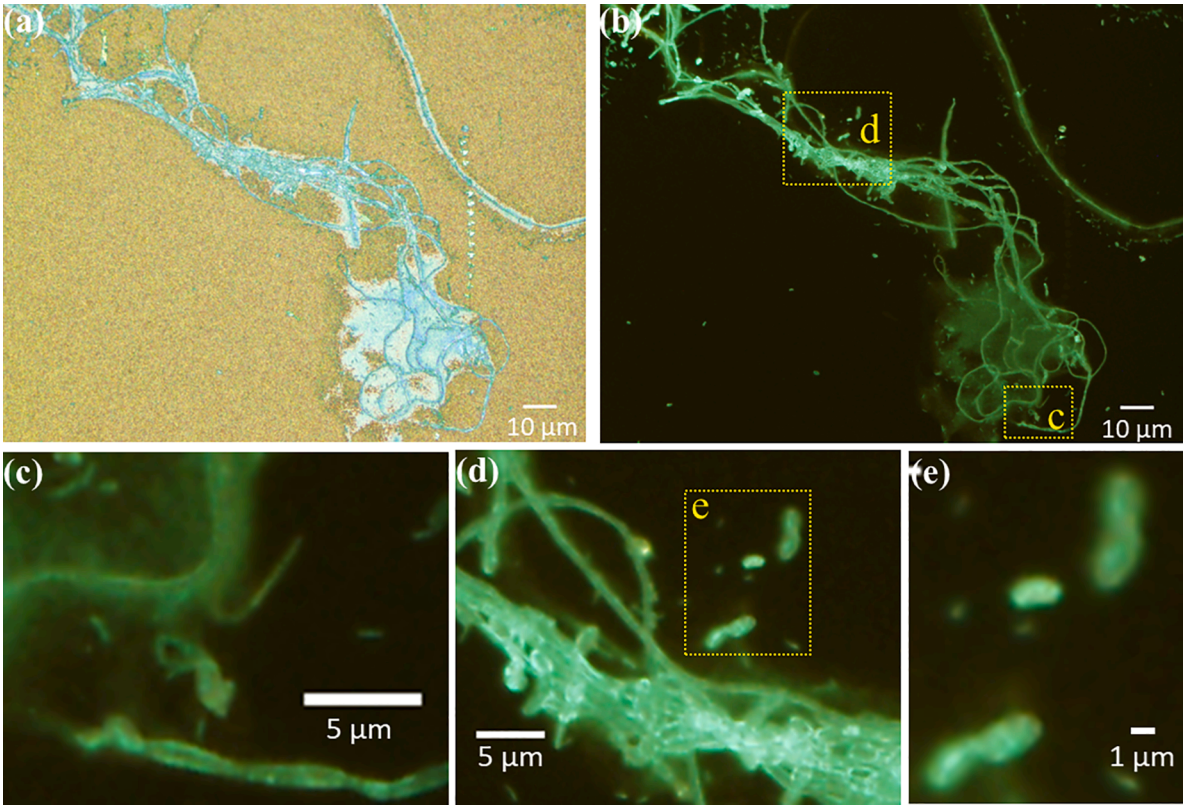


**Fig. 3.** OM reflective image (a) and U-MWBV2 fluorescence images (b-e) of PBAT microplastics placed on a PEF substrate. The PBAT microplastics were those formed during 5 weeks of exposure to Milli-Q water at 23 °C [48].

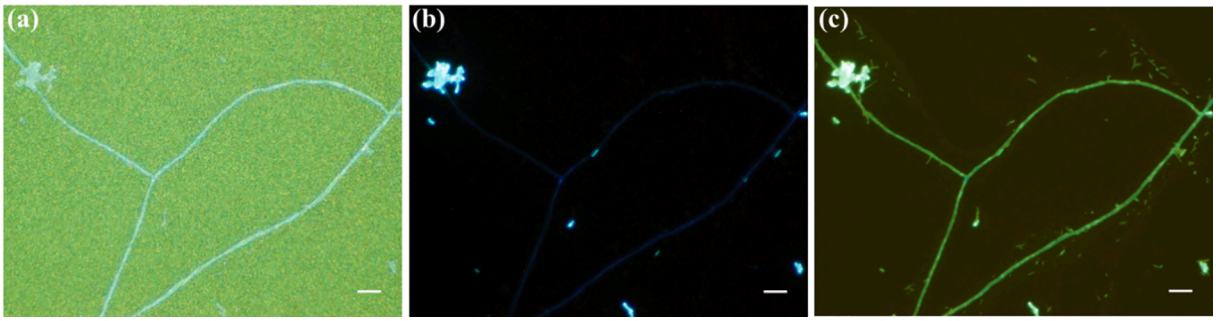


**Fig. 4.** Microscopy images of PBAT microplastics on the PEF substrates: (a) OM reflection (b) U-FUN fluorescence and (c) U-MWBV2 fluorescence. Scale bars are 10 μm long. The PBAT microplastics were those formed during 8 weeks of exposure to MilliQ water at 23 °C [48].

enhancement on the order of 10 – 1000 times [51,52]. Lastly, the surface of gold-coated SiNPs can readily be functionalized to specifically capture certain molecules or particles even within the hot-spots, which has been demonstrated in ref [53].

### 3.2. PEF technique for microplastic detection

Many polymers have intrinsic fluorescent properties, however, most often their intrinsic fluorescence is relatively weak. Here, the intrinsic fluorescence from the pristine PBAT and LDPE plastic films was first examined. Fig. 2a and b show that the regions for fluorescence were located at very low excitation wavelengths (about 200 – 250 nm) for both polymers, and at emission wavelengths of 325 – 500 nm for PBAT and 300 – 550 nm for LDPE. Besides, PBAT shows an additional region for fluorescence at higher excitation wavelengths, around 300 – 350 nm, with emission wavelengths of 325 – 400 nm. This region also reaches up into wavelengths relevant for the employed optical filters in the fluorescence microscope demonstrated below. To further pinpoint these fluorescence microscopy wavelengths, specific fluorescence emission scans for these two plastics with excitations at 360 nm and 400 nm are shown in Fig. 2c and d, respectively. The lowest wavelengths in the intervals, 360 – 370 and 400 – 440 nm, the same as the excitation wavelength region of U-FUN and U-MWBV2 optical filters, respectively, were chosen to minimize scattering disturbance of the spectra. PBAT demonstrated greater fluorescence over LDPE in blue and green for both excitation wavelengths, which can be attributed to the presence of conjugated benzyl groups with delocalized π-electrons and possibly also polarizable ester groups in PBAT polymer chains (see insert in Fig. 2c). Overall, LDPE seemed to have very poor intrinsic fluorescence except within the 200 – 250 nm excitation wavelength (Fig. 2b). However, the emission at this low excitation wavelength demonstrates the potential for blue and green emission if excitation can be enabled for the higher microscopy wavelengths, by for example PEF.

Fig. 3a-e show optical microscope (OM) reflective image and U-

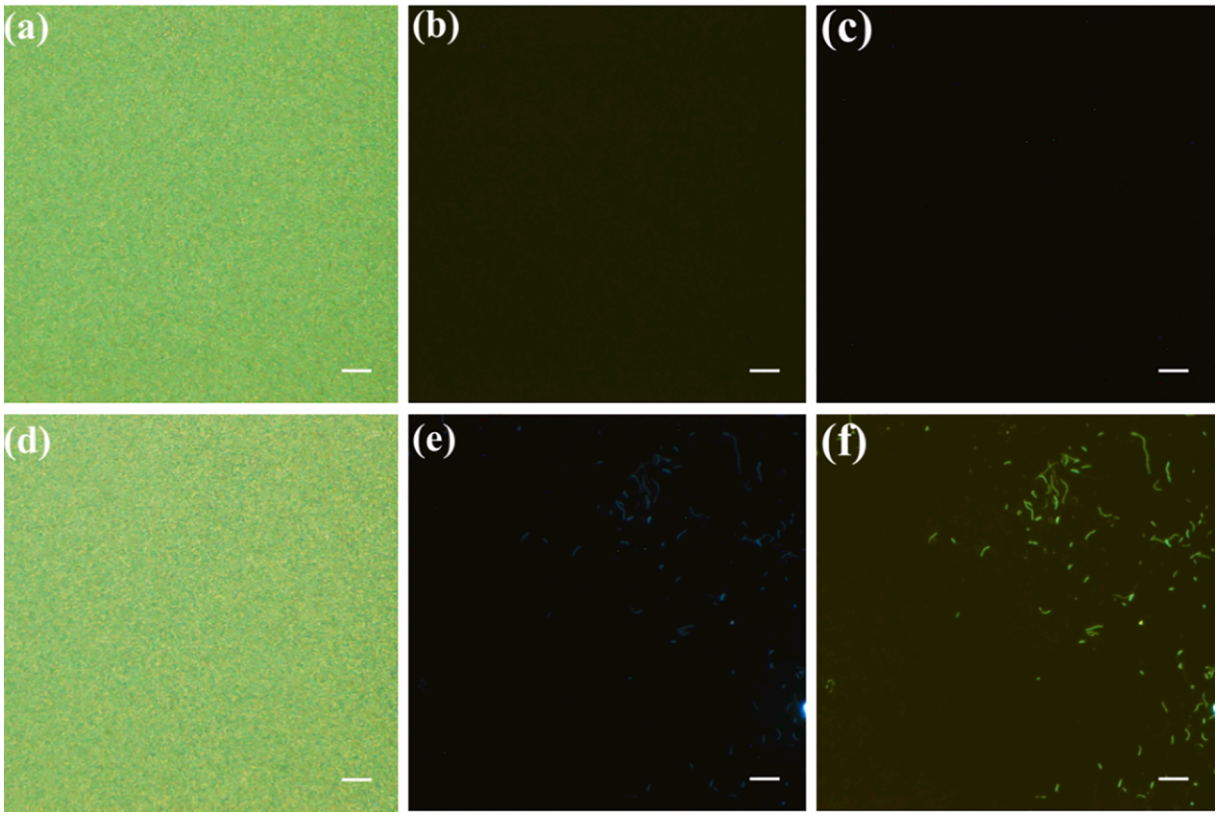


**Fig. 5.** OM reflective (a and d) and fluorescence microscopy U-FUN (b, e) and U-MWBV2 (c, f) images of a blank sample (a, b, c) and LDPE in MilliQ water (d, e, f). The latter represented the LDPE system after 8 weeks exposure to MilliQ water at 23 °C [48]. Scale bars are 10 μm long.

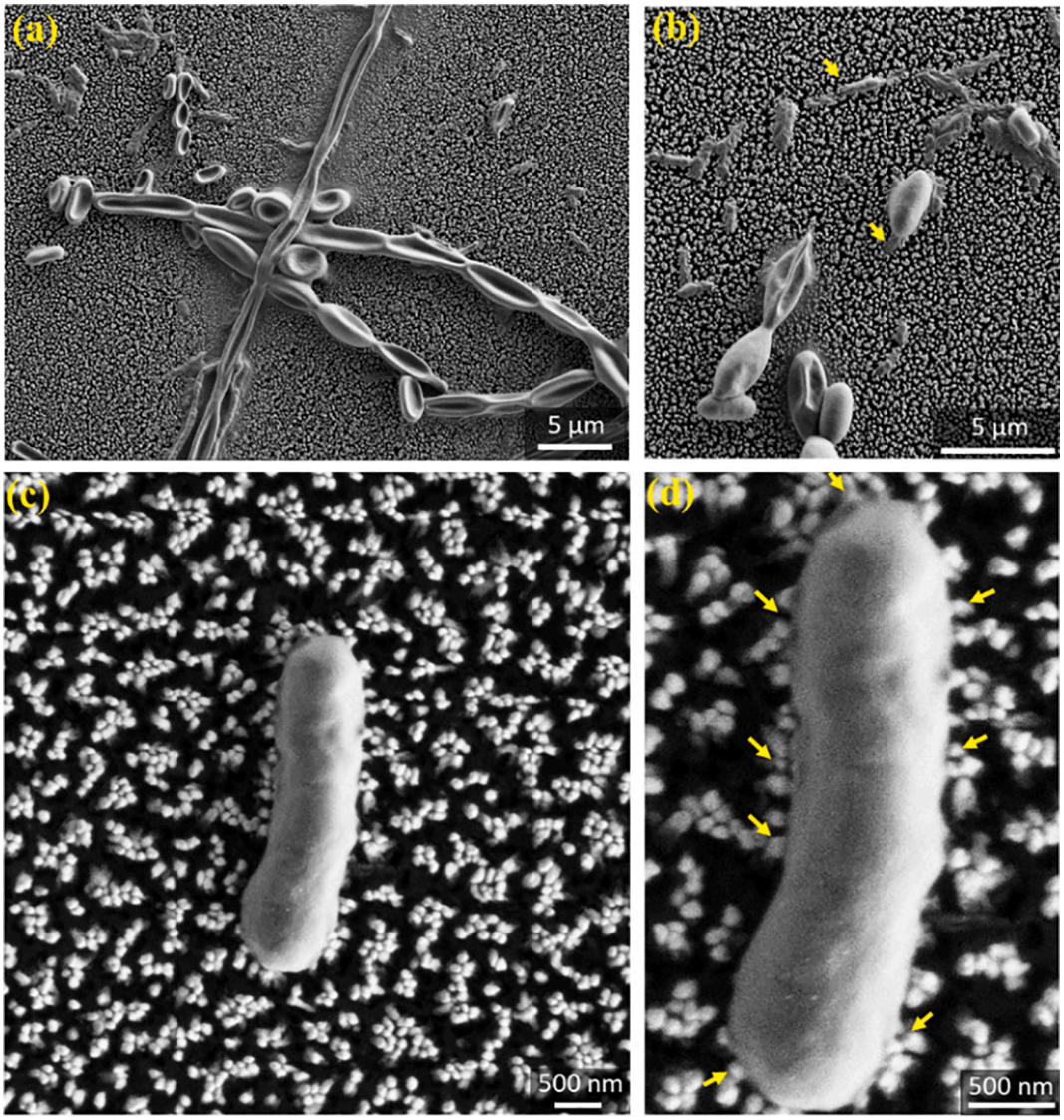


**Fig. 6.** SEM images of PBAT microplastics on the PEF substrates. The PBAT microplastics were those formed during 5 weeks of exposure to MilliQ water at 23 °C [48]. The arrows in b point at microplastics reaching down into the space between the nanopillars, and arrows in d point at the gold nanopillars adhered to the microplastic.

MWBV2 fluorescence images of the PBAT microplastics on the PEF substrates. The PBAT microplastics with different morphologies (fibers, rods, dots, and dissolved (or melted) matter) and different sizes could be clearly observed in the fluorescence microscopy images. Dissolved (or melted) matter refers to the soluble hydrolysis products which were formed during the ageing and solidified within the particle area after water evaporated. The PBAT microplastics fluoresced green under U-MWBV2 fluorescence. In contrast, the reference sample, situated on a glass substrate did not show any fluorescence (not shown). These findings indicated a highly enhanced fluorescence from the AuNP substrates, which made the microplastics visible/observable in fluorescence microscopy, without the need of being stained by fluorescent dyes. The long PBAT microplastic fibers were also observed in the conventional OM (Fig. 3a). However, differently than from the fluorescence images, many of the smaller microplastics were difficult to observe in the OM images.

Fig. 4 shows that the PBAT microplastics fluoresce in blue under the U-FUN optical filter in contrast to green under the U-MWBV2 optical filter. However, the long fibers and many small particles can barely be seen in the OM and the U-FUN cases but are clearly seen in the U-MWBV2 case. A more noticeable example of invisible microplastic particles becoming visible using the PEF substrates can be seen in Fig. 5. The sample (Fig. 5d-f) represented MilliQ water containing LDPE particles formed during 8 weeks of exposure at 23 °C [48]. The images of the blank sample (Fig. 5a-c) show no particles in either the OM or fluorescence images. LDPE sample images show no particles in the OM image, but fiber-like particles of a length of a couple of micrometers are clearly visible in the fluorescence images (Fig. 5d-f). Also here, the U-FUN filter yielded a blue color for the LDPE microplastics with a much lower intensity than with the green color under the U-MWBV2 filter. Hence, it can be concluded that the fluorescence enhancement of the AuNP substrates on both LDPE and PBAT microplastics was greater in U-MWBV2 fluorescence than U-FUN fluorescence.

The microplastics on the PEF substrates were also examined with SEM. As shown in Fig. 6, the PBAT microplastics with different sizes and shapes (fiber, rod, particulate) observed in the fluorescence microscope (Figs. 3 and 4), were also observed/confirmed with SEM; the small rod-like/dot PBAT microplastics were a couple of micrometers long and the microplastic fibers had a diameter of 1–2 µm. Moreover, it could be clearly seen that the microplastics are laying on the PEF substrates after the water evaporates, and some small microplastic particles seem to have a focus near or reaching down into the nanopillar "forest" (Fig. 6a

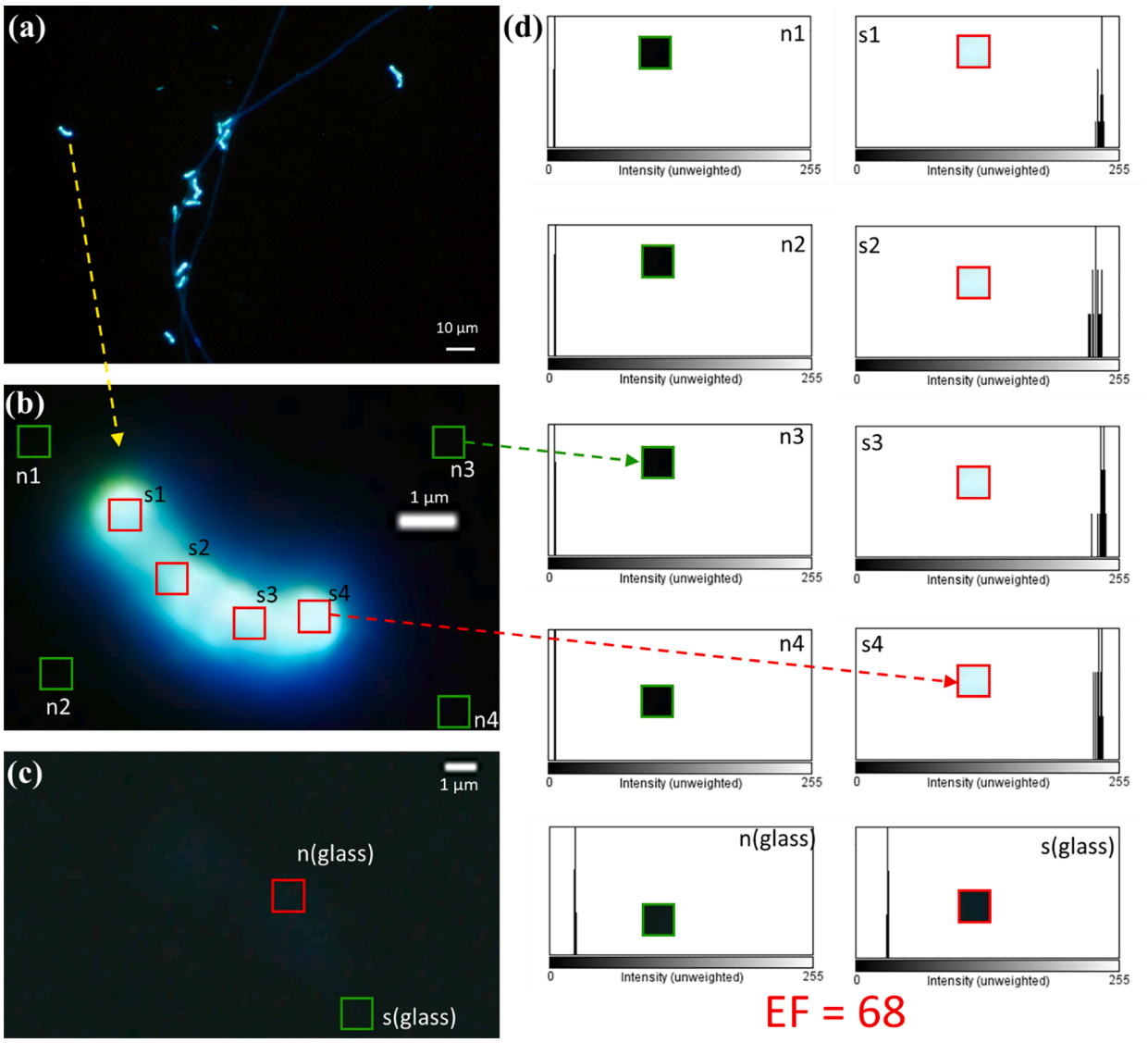


**Fig. 7.** Fluorescence image (U-FUN) of the PBAT microplastic particles on AuNP substrates (a,b) and on a microscope glass slide (c), and (d) histograms of the measured areas within the particle and outside (blank). The microplastic sample was the one formed after 8 weeks of exposure to MilliQ water at 23 °C [48]. A LOD = 0.35 and LOQ = 1.2 femtograms, respectively, were calculated according to standard approximation; three (LOD) and ten (LOQ) times the standard deviation of the blank divided by the linear slope (up to the next concentration level, here signal (s) level). The enhancement factor (EF) was calculated signal-to-noise (S/N) ratios according to $S_{NP}/N_{NP}$ / $S_{Glass}$ /$N_{Glass}$.

and b). Fig. 6c and d show that the nearby nanopillars were drawn towards and adhered tightly to the rod-shaped microplastic particle, forming many nanopillar clusters that mechanically supported the particles. Note that the formed nanopillar clusters lead to the generation of many hot spots with extra high plasmonic fluorescence enhancement [46]. The good adhesion between the microplastic particles and nanopillars, and the formation of supporting nanopillar clusters resulted from the elasto-capillarity effects of the substrates [46].

### 3.3. Detection limits and enhancement factor

For an estimate of detection limits of fluorescence measurements on these substrates, a similar approach as in ref [49] was used. In brief, a well-isolated particle (i.e. with dark background) was chosen (Fig. 7), which showed a fluorescence image (U-FUN filter) was first chosen. A 4x4 pixel area was selected for individual quantifications, to scale well with the size of the particle. Considering that the particle had a 3D-symmetry and that a large part of the particle volume will contribute to the fluorescence signal, the whole volume was considered when determining the total sample mass (this will give a slightly poorer detection limit). Hence, the amount of PBAT in the 4x4x4 pixel was estimated to be 172 femtograms (using a volume of 0.137 µm$^3$ and a density of 1.25 g/cm$^3$), which was used for the detection limit calculation. Based on this, the limit of detection (LOD) was calculated to be 0.35 femtogram and the limit of the quantification (LOQ) became 1.2 femtogram detection, using the U-FUN filter cube and the blue RGB channel. A similar calculation was performed for a PBAT particle on a glass microscope slide for comparison reasons and an enhancement factor of 68 was estimated (Fig. 7). This indicates that the fluorescence enhancement of the gold nanopillar substrates for the PBAT microplastics was 68 times greater than the case of having the microplastics on a glass substrate.

Another example of using this PEF method for improving the detection of microplastics is given in Fig. 8. Artificial seawater droplets containing PBAT microplastics were placed on the PEF substrates, and the salt in seawater crystallized during drying. The microplastic fiber among the salt crystals was clearly revealed in fluorescence microscopy images, while it was hardly seen in the conventional microscopy image. In addition, epoxy microplastics were also tested and they also

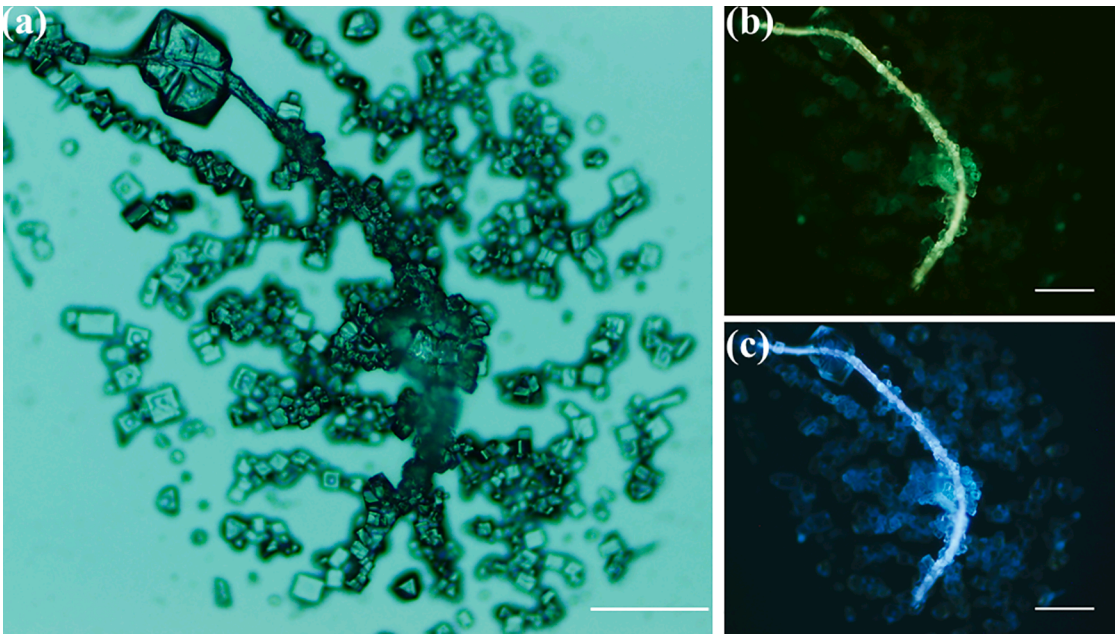


**Fig. 8.** Images of a PBAT fiber among salt crystals; (a) OM image, (b) fluorescence microscopy image using a U-MWBV2 filtercube and (c) fluorescence microscopy image using a U-FUN filtercube. Gold nanopillar substrates are present but are not observed through the layers of salt and the fluorescence enhancement was therefore low. The scale bars are 25 μm long.

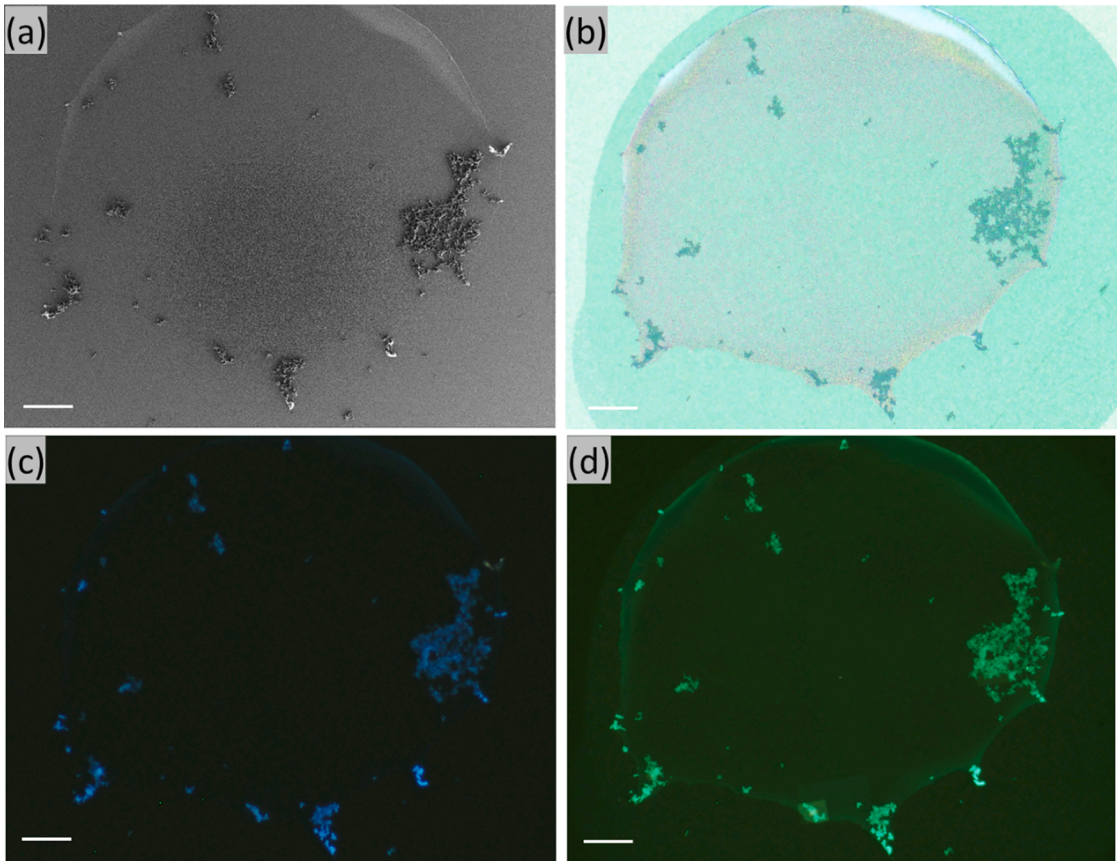


**Fig. 9.** Images of epoxy particles in an evaporated MilliQ water droplet (2 μl); (a) SEM, (b) OM, (c) fluorescence microscopy image using a U-FUN filtercube and (d) fluorescence microscopy image using a U-MWBV2 filtercube. Scale bars are 100 μm.

fluoresced strongly in blue and green in fluorescence microscopy using a U-FUN and U-MWBV2 filtercube, respectively, the same as LDPE and PBAT microplastics (Fig. 9). The result shows that this new method has high potential feasibility for other types of microplastics.

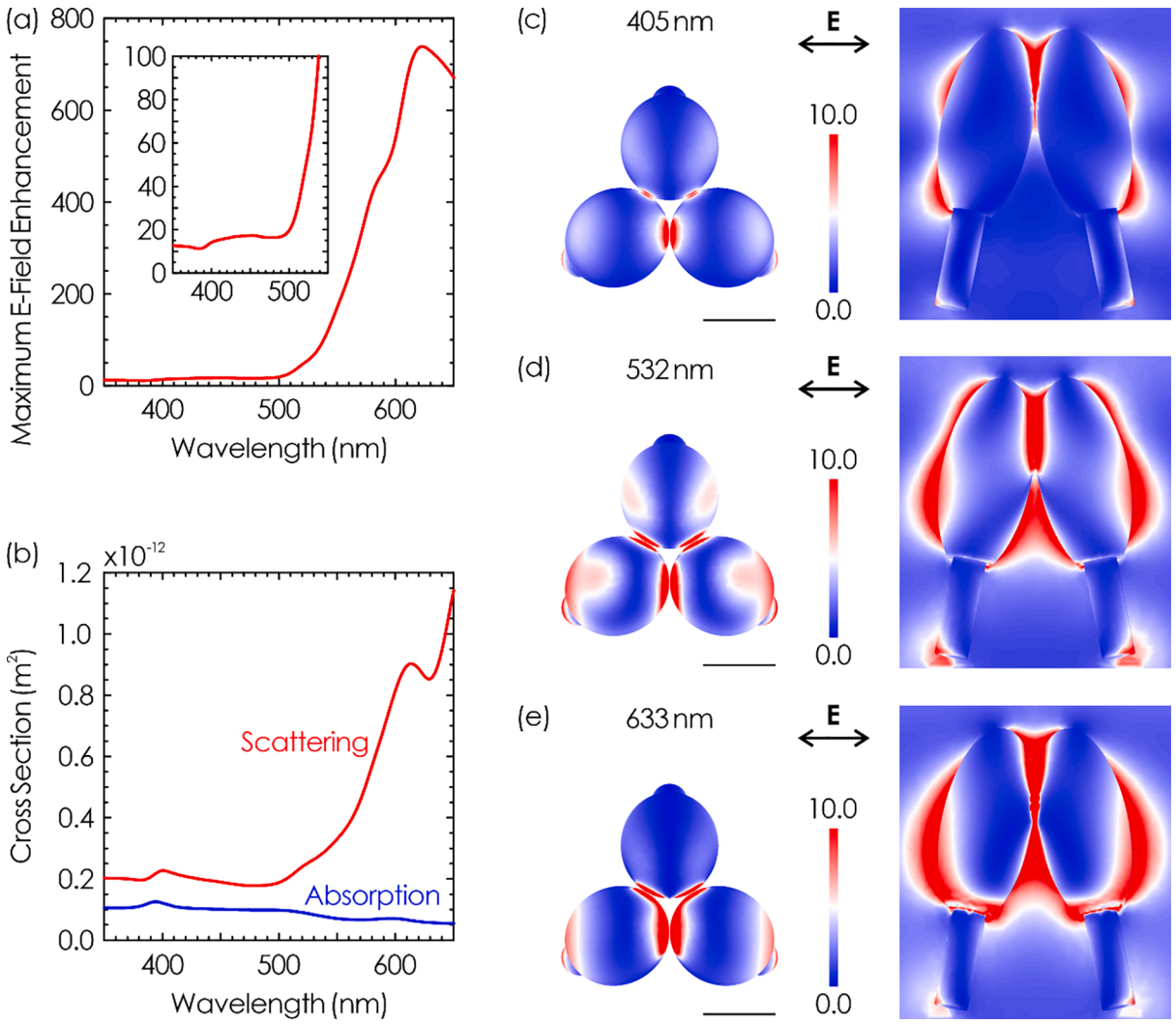


**Fig. 10.** (a) Simulated spectrum of maximum electrical field enhancement for a trimer of gold nanopillars. (b) Simulated spectra of absorption and scattering cross-sections for a trimer of gold nanopillars. (c-e) Distribution of $|E|^2/|E_0|^2$ on the surface of and near a trimer of gold nanopillars. Left: top view showing $|E|^2/|E_0|^2$ on the surface of the nanopillars; Right: side view showing $|E|^2/|E_0|^2$ on the surface of the nanopillars, and in the nearby medium in a cross-sectional cut through the hot spot. Scale bars: 100 nm.

### *3.4. Simulations*

To understand the enhanced fluorescence results, 3D FEM simulations were performed. The electromagnetic enhancement of PEF derives from two parts: I) The near-field enhancement $|E|^2/|E_0|^2$ at the excitation wavelength (where E is enhanced field and $E_0$ is without enhancement); II) The near-field enhancement $|E|^2/|E_0|^2$ across the radiation wavelengths [31]. In other words, the enhanced re-radiated dipolar fields excite the adsorbate, and, if the resulting molecular radiation remains at or near resonance with the enhancing object, the scattered radiation will again be enhanced [31]. Fig. 10a shows the simulated spectrum of maximum $|E|/|E_0|$ near a trimer of gold nanopillars. The maximum $|E|/|E_0|$ lingers around 20 when increasing the wavelength of excitation from 350 to 500 nm, due to loss attributed to the inter-band transition of gold. Further increase of the wavelength of excitation beyond 500 nm dramatically boosted the maximum $|E|/|E_0|$, due to the excitation of strong localized surface-plasmon resonances. The maximum $|E|/|E_0|$ reached ~ 750 at 620 nm excitation. This trend is also shown in Fig. 10b by the simulated scattering spectrum. Since the size of the nanopillars was relatively big, scattering was dominant over absorption, as shown in Fig. 10b. Fig. 10c-e illustrate the distribution of $|E|^2/|E_0|^2$ on the surface of, and near a trimer of gold nanopillars. It can be seen that at 405 nm excitation, the enhanced field was weak and very localized. By increasing the excitation wavelength to 532 and 633 nm, the enhanced field became much stronger, and extended to the nearby medium by tens of nanometers. Therefore, referring to the greenish fluorescent image of the microplastics, it can be concluded that the major contribution to the observed enhanced fluorescence was the near-field enhancement across the radiation wavelengths. Furthermore, near the excitation wavelengths, the maximum electrical field enhancement was ~ 12 with the U-FUN filter (360 – 370 nm excitation) and ~ 20 with the U-MWBV2 filter (400 – 440 nm excitation). Although near-field enhancement at the excitation wavelengths (UV-blue) played a minor role in the overall fluorescence enhancement as shown in Fig. 10(a), it also contributed to the greater fluorescence enhancement with U-MWBV2 filter than with the U-FUN filter (Figs. 4 and 5). Besides, the simulation results suggest that a much greater fluorescence enhancement of PEF on microplastics will be obtained if an excitation filter over BP 500 nm is used in fluorescence microscopy, i.e., if the microplastic at hand has a fluorescence to enhance in the relevant wavelength range.

## 4. Conclusions

In this study, the concept of plasmonic-enhanced fluorescence was,

for the first time, employed to enhance the fluorescence signal of microplastics with the goal to develop a new microplastic detection method. Gold coated silicon nanopillar substrates with strong electromagnetic field enhancement properties were tested as an analytical tool for the detection of undyed microplastics in a fluorescence microscope. Due to the remarkable fluorescence enhancement by the AuNP substrates, both LDPE and PBAT microplastics that have low intrinsic fluorescent properties became visible/detectable, even particles completely invisible in conventional light microscopy. Both PBAT and LDPE microplastics on the PEF substrates fluoresced most strongly in green when excitated with 400 – 440 nm wavelength, where the weak intrinsic green fluorescence likely is scattering enhanced by the PEF substrate. The estimated fluorescence enhancement factor on the PBAT microplastics reached a value close to 70. Epoxy microplastics also fluoresced strongly using the PEF substrates. Simulations indicated that the major contribution to the observed enhanced fluorescence was the near-field enhancement across the radiation wavelengths. Apart from fluorescence enhancement, the substrates showed additional advantages, for improved detection of microplastics in dilute water samples, such as superhydrophobicity and high adhesion to sample droplets.

## Declaration of Competing Interest

The authors declare that they have no known competing financial interests or personal relationships that could have appeared to influence the work reported in this paper.

## Acknowledgments

The financial support from the Swedish Environmental Protection Agency (project: NV-06547-19) is gratefully acknowledged. T. Rindzevicius acknowledges the financial support from the European Union's Horizon 2020 research and innovation program under grant agreement no. 883390 (H2020-SU-SECU-2019 SERSing Project), the Danish National Research Foundation (DNRF122), the Villum Fonden (grant no. 9301) for Intelligent Drug Delivery and Sensing Using Microcontainers and Nanomechanics (IDUN), and the BioInnovation Institute Foundation for Therapeutic Drug Monitoring (grant no. NNF20SA0063552). K. Wu acknowledges Double First-Class University Construction Fund from Shanghai Jiao Tong University (WH220403011).

## References

[1] R.U. Halden, C. Rolsky, F.R. Khan, Time: A Key Driver of Uncertainty When Assessing the Risk of Environmental Plastics to Human Health, Environ. Sci. Technol. 55 (19) (2021) 12766–12769, https://doi.org/10.1021/acs.est.1c02580.
[2] R. Geyer, J.R. Jambeck, K.L. Law, Production, use, and fate of all plastics ever made, Sci. Adv. 3 (7) (2017), e1700782.
[3] A.L.P. Silva, J.C. Prata, T.R. Walker, A.C. Duarte, W. Ouyang, D. Barcelò, T. Rocha-Santos, Increased plastic pollution due to COVID-19 pandemic: Challenges and recommendations, Chem. Eng. J. 405 (2021), 126683.
[4] S. Sharma, S. Basu, N.P. Shetti, M.N. Nadagouda, T.M. Aminabhavi, Microplastics in the environment: Occurrence, perils, and eradication, Chem. Eng. J. 408 (2021), 127317.
[5] C. Ostle, R.C. Thompson, D. Broughton, L. Gregory, M. Wootton, D.G. Johns, The rise in ocean plastics evidenced from a 60-year time series, Nat. Commun. 10 (1) (2019) 1–6.
[6] K. Min, J.D. Cuiffi, R.T. Mathers, Ranking environmental degradation trends of plastic marine debris based on physical properties and molecular structure, Nat. Commun. 11 (1) (2020) 1–11.
[7] X.-F. Wei, F. Nilsson, H. Yin, M.S. Hedenqvist, Microplastics Originating from Polymer Blends: An Emerging Threat? Environ. Sci. Technol. 55 (8) (2021) 4190–4193, https://doi.org/10.1021/acs.est.1c00588.
[8] S.T. Sait, L. Sørensen, S. Kubowicz, K. Vike-Jonas, S.V. Gonzalez, A. G. Asimakopoulos, A.M. Booth, Microplastic fibres from synthetic textiles: Environmental degradation and additive chemical content, Environ. Pollut. 268 (2021), 115745.
[9] A. Collignon, J.-H. Hecq, F. Glagani, P. Voisin, F. Collard, A. Goffart, Neustonic microplastic and zooplankton in the North Western Mediterranean Sea, Mar. Pollut. Bull. 64 (4) (2012) 861–864.
[10] A.A. Koelmans, N.H. Mohamed Nor, E. Hermsen, M. Kooi, S.M. Mintenig, J. De France, Microplastics in freshwaters and drinking water: Critical review and assessment of data quality, Water Res. 155 (2019) 410–422, https://doi.org/10.1016/j.watres.2019.02.054.
[11] I.V. Kirstein, F. Hensel, A. Gomiero, L. Iordachescu, A. Vianello, H.B. Wittgren, J. Vollertsen, Drinking plastics? – Quantification and qualification of microplastics in drinking water distribution systems by μFTIR and Py-GCMS, Water Res. 188 (2021), 116519, https://doi.org/10.1016/j.watres.2020.116519.
[12] A. Ragusa, A. Svelato, C. Santacroce, P. Catalano, V. Notarstefano, O. Carnevali, F. Papa, M.C.A. Rongioletti, F. Baiocco, S. Draghi, Plasticenta: First evidence of microplastics in human placenta, Environ. Int. 146 (2021), 106274.
[13] F. Bessa, N. Ratcliffe, V. Otero, P. Sobral, J.C. Marques, C.M. Waluda, P.N. Trathan, J.C. Xavier, Microplastics in gentoo penguins from the Antarctic region, Sci. Rep. 9 (1) (2019) 1–7.
[14] S. Wolff, J. Kerpen, J. Prediger, L. Barkmann, L. Müller, Determination of the microplastics emission in the effluent of a municipal waste water treatment plant using Raman microspectroscopy, Water Res. X 2 (2019), 100014.
[15] X.F. Wei, A.J. Capezza, Y. Cui, L. Li, A. Hakonen, B. Liu, M.S. Hedenqvist, Millions of microplastics released from a biodegradable polymer during biodegradation/enzymatic hydrolysis, Water Res. 211 (2022), 118068, https://doi.org/10.1016/j.watres.2022.118068.
[16] V.P. Ranjan, A. Joseph, S. Goel, Microplastics and other harmful substances released from disposable paper cups into hot water, J. Hazard. Mater. 404 (2020), 124118.
[17] A.L. Andrady, The plastic in microplastics: A review, Mar. Pollut. Bull. 119 (1) (2017) 12–22.
[18] M. Jang, W.J. Shim, Y. Cho, G.M. Han, Y.K. Song, S.H. Hong, A close relationship between microplastic contamination and coastal area use pattern, Water Res. 171 (2020) 115400.
[19] S. Wagner, T. Huffer, P. Klockner, M. Wehrhahn, T. Hofmann, T. Reemtsma, Tire wear particles in the aquatic environment - A review on generation, analysis, occurrence, fate and effects, Water Res. 139 (2018) 83–100, https://doi.org/10.1016/j.watres.2018.03.051.
[20] M.C.M. Blettler, E. Abrial, F.R. Khan, N. Sivri, L.A. Espinola, Freshwater plastic pollution: Recognizing research biases and identifying knowledge gaps, Water Res. 143 (2018) 416–424, https://doi.org/10.1016/j.watres.2018.06.015.
[21] F. Wang, C.S. Wong, D. Chen, X.W. Lu, F. Wang, E.Y. Zeng, Interaction of toxic chemicals with microplastics: A critical review, Water Res. 139 (2018) 208–219, https://doi.org/10.1016/j.watres.2018.04.003.
[22] G. Xu, H. Cheng, R. Jones, Y. Feng, K. Gong, K. Li, X. Fang, M.A. Tahir, V.K. Valev, L. Zhang, Surface-Enhanced Raman Spectroscopy Facilitates the Detection of Microplastics< 1 μm in the Environment, Environ. Sci. Technol. (2020).
[23] P. Pannetier, J. Cachot, C. Clérandeau, F. Faure, K. Van Arkel, L.F. de Alencastro, C. Levasseur, F. Sciacca, J.-P. Bourgeois, B. Morin, Toxicity assessment of pollutants sorbed on environmental sample microplastics collected on beaches: Part I-adverse effects on fish cell line, Environ. Pollut. 248 (2019) 1088–1097.
[24] E. Agathokleous, I. Iavicoli, D. Barceló, E.J. Calabrese, Ecological risks in a 'plastic'world: A threat to biological diversity? J. Hazard. Mater. 417 (2021) 126035.
[25] W. Zhang, Z.Q. Dong, L. Zhu, Y.Z. Hou, Y.P. Qiu, Direct Observation of the Release of Nanoplastics from Commercially Recycled Plastics with Correlative Raman Imaging and Scanning Electron Microscopy, ACS Nano 14 (7) (2020) 7920–7926, https://doi.org/10.1021/acsnano.0c02878.
[26] S. Huppertsberg, T.P. Knepper, Instrumental analysis of microplastics—benefits and challenges, Anal. Bioanal. Chem. 410 (25) (2018) 6343–6352.
[27] W.J. Shim, S.H. Hong, S.E. Eo, Identification methods in microplastic analysis: a review, Anal. Methods 9 (9) (2017) 1384–1391.
[28] S. Jung, S.-H. Cho, K.-H. Kim, E.E. Kwon, Progress in Quantitative Analysis of Microplastics in the Environment: A Review, Chem. Eng. J. 422 (2021) 130154.
[29] T. Maes, R. Jessop, N. Wellner, K. Haupt, A.G. Mayes, A rapid-screening approach to detect and quantify microplastics based on fluorescent tagging with Nile Red, Sci. Rep. 7 (1) (2017) 1–10.
[30] G. Erni-Cassola, M.I. Gibson, R.C. Thompson, J.A. Christie-Oleza, Lost, but found with Nile red: a novel method for detecting and quantifying small microplastics (1 mm to 20 μm) in environmental samples, Environ. Sci. Technol. 51 (23) (2017) 13641–13648.
[31] J.-F. Li, C.-Y. Li, R.F. Aroca, Plasmon-enhanced fluorescence spectroscopy, Chem. Soc. Rev. 46 (13) (2017) 3962–3979, https://doi.org/10.1039/C7CS00169J.
[32] A.M. Glass, P.F. Liao, J.G. Bergman, D.H. Olson, Interaction of metal particles with adsorbed dye molecules: absorption and luminescence, Opt. Lett. 5 (9) (1980) 368–370, https://doi.org/10.1364/OL.5.000368.
[33] K. Yang, X. Yin, Y. Yan, K. Yang, P. Pi, S. Xu, J. Fang, Q. Li, X. Wen, An aqueous gold nanorod and CdSe quantum dots hybrid nanomaterial: A potential plasmon enhanced fluorescence structure for bio-probe fabrication, Chem. Eng. J. 426 (2021), 131571, https://doi.org/10.1016/j.cej.2021.131571.
[34] M. Bauch, K. Toma, M. Toma, Q. Zhang, J. Dostalek, Plasmon-Enhanced Fluorescence Biosensors: a Review, Plasmonics 9 (4) (2014) 781–799, https://doi.org/10.1007/s11468-013-9660-5.
[35] J. Dong, Z. Zhang, H. Zheng, M. Sun, Recent Progress on Plasmon-Enhanced Fluorescence, Nanophotonics 4 (4) (2015) 472–490, https://doi.org/10.1515/nanoph-2015-0028.
[36] M. Ramírez-Maureira, V.V. C, A. Riveros, P.J.G. Goulet, I.O. Osorio-Román, Shell-isolated nanoparticle-enhanced fluorescence (SHINEF) of CdTe quantum dots, Mater. Chem. Phys. 151 (2015) 351-356. 10.1016/j.matchemphys.2014.12.003.
[37] W.E. Martin, B.R. Srijanto, C.P. Collier, T. Vosch, C.I. Richards, A Comparison of Single-Molecule Emission in Aluminum and Gold Zero-Mode Waveguides, J. Phys. Chem. A 120 (34) (2016) 6719–6727, https://doi.org/10.1021/acs.jpca.6b03309.

[38] H. Lee, W.J. Rhee, G. Moon, S. Im, T. Son, J.-S. Shin, D. Kim, Plasmon-enhanced fluorescence correlation spectroscopy for super-localized detection of nanoscale subcellular dynamics, Biosens. Bioelectron. 184 (2021), 113219, https://doi.org/10.1016/j.bios.2021.113219.
[39] N.T. Emerson, H. Yang, Reproducibly Measuring Plasmon-Enhanced Fluorescence in Bulk Solution Across a 20-Fold Range of Optical Densities, Anal. Chem. 93 (22) (2021) 8045–8053, https://doi.org/10.1021/acs.analchem.1c01210.
[40] M. Fleischmann, P.J. Hendra, A.J. McQuillan, Raman spectra of pyridine adsorbed at a silver electrode, Chem. Phys. Lett. 26 (2) (1974) 163–166, https://doi.org/10.1016/0009-2614(74)85388-1.
[41] J. Langer, D.J. de Aberasturi, J. Aizpurua, R.A. Alvarez-Puebla, B. Auguie, J. J. Baumberg, G.C. Bazan, S.E.J. Bell, A. Boisen, A.G. Brolo, J. Choo, D. Cialla-May, V. Deckert, L. Fabris, K. Faulds, F.J.G. de Abajo, R. Goodacre, D. Graham, A. J. Haes, C.L. Haynes, C. Huck, T. Itoh, M. Ka, J. Kneipp, N.A. Kotov, H. Kuang, E. C. Le Ru, H.K. Lee, J.F. Li, X.Y. Ling, S.A. Maier, T. Mayerhofer, M. Moskovits, K. Murakoshi, J.M. Nam, S. Nie, Y. Ozaki, I. Pastoriza-Santos, J. Perez-Juste, J. Popp, A. Pucci, S. Reich, B. Ren, G.C. Schatz, T. Shegai, S. Schlucker, L.L. Tay, K. G. Thomas, Z.Q. Tian, R.P. Van Duyne, T. Vo-Dinh, Y. Wang, K.A. Willets, C. Xu, H. Xu, Y. Xu, Y.S. Yamamoto, B. Zhao, L.M. Liz-Marzan, Present and Future of Surface-Enhanced Raman Scattering, ACS Nano 14 (1) (2020) 28–117, https://doi.org/10.1021/acsnano.9b04224.
[42] J. Shan, Y. Zhang, J. Wang, T. Ren, M. Jin, X. Wang, Microextraction based on microplastic followed by SERS for on-site detection of hydrophobic organic contaminants, an indicator of seawater pollution, J. Hazard. Mater. 400 (2020), 123202.
[43] L. Lv, L. He, S. Jiang, J. Chen, C. Zhou, J. Qu, Y. Lu, P. Hong, S. Sun, C. Li, In situ surface-enhanced Raman spectroscopy for detecting microplastics and nanoplastics in aquatic environments, Sci. Total Environ. 728 (2020) 138449.
[44] M.S. Schmidt, J. Hübner, A. Boisen, Large Area Fabrication of Leaning Silicon Nanopillars for Surface Enhanced Raman Spectroscopy, Adv. Mater. 24 (10) (2012) OP11-OP18, https://doi.org/10.1002/adma.201103496.
[45] K. Wu, T. Rindzevicius, M.S. Schmidt, K.B. Mogensen, A. Hakonen, A. Boisen, Wafer-Scale Leaning Silver Nanopillars for Molecular Detection at Ultra-Low Concentrations, J. Phys. Chem. C 119 (4) (2015) 2053–2062, https://doi.org/10.1021/jp510073y.
[46] A. Hakonen, T. Rindzevicius, M.S. Schmidt, P.O. Andersson, L. Juhlin, M. Svedendahl, A. Boisen, M. Käll, Detection of nerve gases using surface-enhanced Raman scattering substrates with high droplet adhesion, Nanoscale 8 (3) (2016) 1305–1308.
[47] A. Hakonen, F. Wang, P.O. Andersson, H. Wingfors, T. Rindzevicius, M.S. Schmidt, V.R. Soma, S. Xu, Y. Li, A. Boisen, H. Wu, Hand-Held Femtogram Detection of Hazardous Picric Acid with Hydrophobic Ag Nanopillar SERS Substrates and Mechanism of Elasto-Capillarity, ACS Sensors 2 (2) (2017) 198–202, https://doi.org/10.1021/acssensors.6b00749.
[48] X.-F. Wei, M. Bohlén, C. Lindblad, M. Hedenqvist, A. Hakonen, Microplastics generated from a biodegradable plastic in freshwater and seawater, Water Res. (2021), 117123, https://doi.org/10.1016/j.watres.2021.117123.
[49] A. Hakonen, M. Svedendahl, R. Ogier, Z.-J. Yang, K. Lodewijks, R. Verre, T. Shegai, P.O. Andersson, M. Käll, Dimer-on-mirror SERS substrates with attogram sensitivity fabricated by colloidal lithography, Nanoscale 7 (21) (2015) 9405–9410, https://doi.org/10.1039/C5NR01654A.
[50] P.B. Johnson, R.W. Christy, Optical Constants of the Noble Metals, Phys. Rev. B 6 (12) (1972) 4370–4379, https://doi.org/10.1103/PhysRevB.6.4370.
[51] J.R. Lakowicz, Radiative decay engineering 5: metal-enhanced fluorescence and plasmon emission, Anal. Biochem. 337 (2) (2005) 171–194, https://doi.org/10.1016/j.ab.2004.11.026.
[52] A. Hakonen, Plasmon Enhancement and Surface Wave Quenching for Phase Ratiometry in Coextraction-Based Fluorosensors, Anal. Chem. 81 (11) (2009) 4555–4559, https://doi.org/10.1021/ac8025866.
[53] L. Juhlin, T. Mikaelsson, A. Hakonen, M.S. Schmidt, T. Rindzevicius, A. Boisen, M. Käll, P.O. Andersson, Selective surface-enhanced Raman scattering detection of Tabun, VX and Cyclosarin nerve agents using 4-pyridine amide oxime functionalized gold nanopillars, Talanta 211 (2020), 120721, https://doi.org/10.1016/j.talanta.2020.120721.